Journal of Power Sources 185 (2008) 1444–1453

Contents lists available at ScienceDirect

Journal of Power Sources

journal homepage: www.elsevier.com/locate/jpowsour

Cycle life evaluation of 3 Ah $Li_xMn_2O_4$-based lithium-ion secondary cells for low-earth-orbit satellites
I. Full cell results

Shelley Brown[a,*], Keita Ogawa[b], Youichi Kumeuchi[c], Shinsuke Enomoto[c], Masatoshi Uno[d], Hirobumi Saito[d], Yoshitsugu Sone[d], Daniel Abraham[e], Göran Lindbergh[a]

[a] School of Chemical Science and Engineering, Department of Chemical Engineering and Technology, Teknikringen 42, Royal Institute of Technology, Stockholm SE-100 44, Sweden
[b] Advanced Engineering Services Co., Ltd., 1-6-1 Takezono, Tsukuba, Ibaraki 305-0032, Japan
[c] NEC-Tokin Corporation, 1120 Shimokuzawa, Sagamihara, Kanagawa 229-1198, Japan
[d] Japan Aerospace Exploration Agency, Institute of Space and Astronautical Science, 3-1-1 Yoshinodai, Sagamihara, Kanagawa 229-8510, Japan
[e] Chemical Engineering Division, Argonne National Laboratory, 9700 South Cass Avenue, Argonne, IL 60439, USA

ARTICLE INFO

Article history:
Received 11 May 2008
Received in revised form 6 July 2008
Accepted 13 July 2008
Available online 5 August 2008

Keywords:
Lithium-ion
LEO satellite
Ageing

ABSTRACT

Lithium-ion batteries are a candidate for the energy storage system onboard low-earth-orbit satellites. Cycle life performance under both orbital and terrestrial conditions must be investigated in order to evaluate any inadvertent effects due to the former and the validity of the latter, with a successful comparison allowing for the extension of terrestrial experimental matrices in order to identify the effects of ageing. The orbital performance of $Li_xMn_2O_4$-based pouch cells onboard the microsatellite REIMEI was monitored and compared with terrestrial experiments, with the cells found to be unaffected by orbital conditions. A lifetime matrix of different cycling depths-of-discharge (DODs: 0, 20, 40%) and temperatures (25, 45 °C) was undertaken with periodic reference performance tests. A decrease in both the cell end-of-discharge cycling voltage and capacity was accelerated by both higher temperatures and larger DODs. Impedance spectra measured for all ageing conditions indicated that the increase was small, manifested in a state-of-charge dependent increase of the high-frequency semi-circle and a noticeable increase in the high-frequency real axis intercept. An evaluation of the change of both the resistance and capacity of 3 Ah cells led to the development of a potential prognostic state-of-health indicator. The use of elevated temperatures to accelerate cell ageing was validated.

1. Introduction

Advanced battery technologies that have higher gravimetric and volumetric energy densities, longer cycle life and better rate capability can result in either the increase of a satellite payload [1] or enable the use of microsatellites (i.e. piggy-back satellites). Microsatellites (~10–100 kg [2]) operate in a low-earth-orbit (LEO, 500–1000 km above the earth) and provide affordable and frequent opportunities for short-term (typically less than 1 year) missions. State-of-the-art nickel-based (e.g. nickel metal hydride, nickel cadmium) systems that have typically been used for LEO satellites have a specific energy of 40–60 Wh kg^{-1} and account for approximately 10% of the total satellite mass [2,3]. Lithium-ion batteries are an attractive candidate for LEO satellites due to the higher energy density, higher working voltage, lower self-discharge and potentially greater configuration flexibility with laminated cell packaging [2]. A satellite in LEO typically experiences 65 min of sunshine during which time the battery is recharged via the solar cells, followed by 35 min of eclipse where the battery meets the electrical demands of the mission. In order to achieve a 5 year LEO mission life (30 000 cycles without interruption), lithium-ion cells must be operated under moderate conditions including a shallow depth of discharge (typically between 20 and 40%) and in a reasonable temperature range (10–25 °C) [1–10]. Of key interest to satellite power systems engineers is how to manage a particular lithium-ion battery chemistry, with a specific cell design, in order to maximise the cycle life.

One of the candidate lithium-ion technologies for LEO satellites utilises a manganese spinel intercalation material as the active component of the porous positive electrode. In comparison with other typical positive electrode materials, manganese spinel is one of the most promising because it is inexpensive, has acceptable

* Corresponding author. Tel.: +46 8 7908143; fax: +46 8 108087.
E-mail address: shelleyb@kth.se (S. Brown).

0378-7753/$ – see front matter © 2008 Elsevier B.V. All rights reserved.
doi:10.1016/j.jpowsour.2008.07.070

environmental characteristics and good safety [11]. Despite the improvement in the room temperature cycle life performance of state-of-the-art $Li_xMn_2O_4$-based lithium-ion batteries, this battery chemistry has received little attention from the space industry for missions, with only one published study on the lifetime performance of 14.6 Ah $Li_xMn_2O_4$battery for LEO satellites [8]. This reluctance by the space industry could be due to the problem of capacity fade at elevated temperatures [12]. Unlike electronic devices and stationary vehicles where the temperature can typically rise to 50 °C, the temperature of a lithium-ion battery onboard a LEO satellite can be maintained between 20 and 25 °C, therefore a battery that has a low capacity fade at room temperature would be suitable. However, in order to accelerate the capacity fade of a lithium-ion battery to gauge expected lifetime performance under a specific LEO load, elevated temperatures must be studied and the resulting degradation investigated to ensure that the effects of ageing are the same regardless of the accelerating condition.

The operation of a lithium-ion battery onboard a LEO satellite provides a set of unique conditions, namely, that the battery is subjected to a specific load cycle and temperature, with both variables monitored from a control room on earth. This differs significantly from terrestrial applications where the lithium-ion battery is both operated under unpredictable conditions, for example, hybrid electric vehicles, and is difficult to monitor in the field for extended periods of time. These unique LEO satellite conditions provide an excellent opportunity for battery engineers to do the following: (1) undertake terrestrial experimental simulations on the battery (reflecting the conditions onboard the LEO satellite) and compare the performance with orbital data, (2) on the basis that the terrestrial and orbital performance data are similar, terrestrial simulations can be undertaken with periodic reference performance tests to monitor cell capacity fade and impedance increase, and (3) combine battery performance data with the results of electrochemical measurements of individual electrodes harvested from aged batteries and discern the effects of ageing contributing to both capacity fade and impedance increase. Understanding the performance of a lithium-ion battery onboard a LEO satellite is envisaged as being an important step in both improving the design of the battery chemistry and developing a state-of-health (SOH) indication scheme.

In this study, the terrestrial and orbital lifetime performance of commercial 3 Ah laminated pouch cells, based on $Li_xMn_2O_4$technology (NEC-Tokin), has been studied as a part of a Japan Aerospace Exploration Agency (JAXA) program to demonstrate the use of lithium-ion batteries onboard LEO microsatellites. Firstly, a battery pack was developed for the microsatellite REIMEI (~70 kg, launched August 2005, formerly known as INDEX) and both the end-of-discharge-voltage (EODV) and temperature were monitored from a control room on earth. Secondly, pre-launch experimental simulation of a battery cell and an identical copy of the launched battery pack, under the forecasted cycling and temperature conditions onboard REIMEI, was undertaken and continued during the duration of the mission. Subsequently, the terrestrial and orbital EODV performance as a function of cycle number was compared. Thirdly, cells were subjected to ageing according to a predefined lifetime matrix that included two accelerating factors: (1) temperature (25, 45 °C), and (2) cycling depth of discharge (20, 40%). The measurements were complemented with calendar life tests of fully charged cells under float conditions. Part one of this two part series evaluates the performance of the lithium-ion battery pack in orbit and examines the cell lifetime data in order to identify: (1) the effect of both depth-of-discharge and temperature on capacity fade and impedance increase with increasing cycle number, and (2) probe possible SOH schemes. Part two details the electrochemical examination of electrodes harvested from aged cells that were taken off testing at specified points in time.

Table 1
3 Ah pouch cell design

Electrode	
Positive active material	$Li_xMn_2O_4$-based
Positive current collector material	Al
Negative active material	graphite-based
Negative current collector material	Cu
Electrolyte	1 M $LiPF_6$EC/DEC(3:7 by wt%) + additives
Rated capacity	3 Ah
Weight	75 g
Dimension	145 mm × 80 mm × 4 mm
Energy density	
Mass	158 Wh kg^{-1}
Volume	340 Wh L^{-1}
Charge voltage	4.1 V (4.2 V)
Lower voltage limit	3.0 V

2. Experimental

2.1. Battery design and operation onboard REIMEI

The details of the 3 Ah commercial (supplied by NEC-Tokin) pouch cells are given in Table 1 and a picture of a cell shown in Fig. 1(a). The double-sided positive electrode, consisting of a mixture of active $Li_xMn_2O_4$-based material, carbon additives and binder coated onto an aluminium current collector, was encased in a separator envelope and sandwiched between double-sided

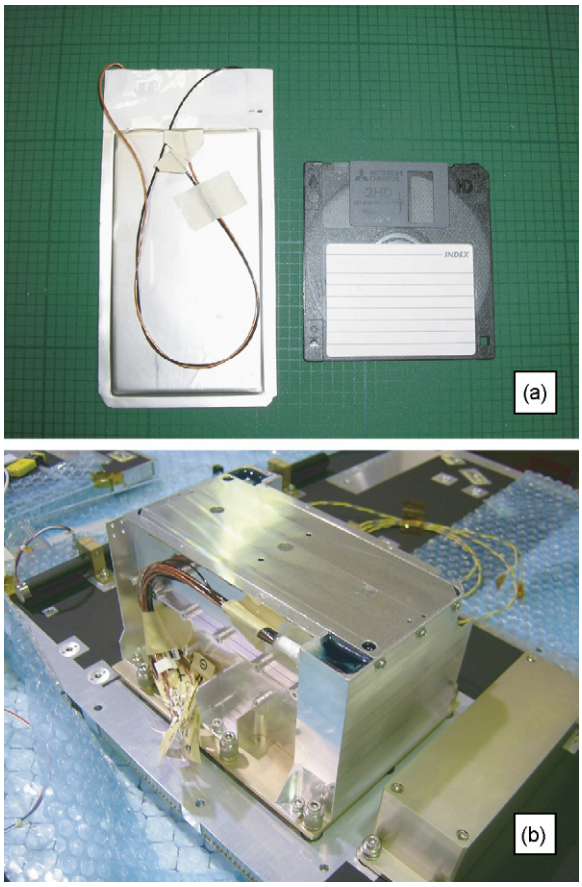

Fig. 1. (a) 3 Ah pouch cell and (b) REIMEI battery.

Table 2
REIMEI battery design

Configuration	7 Cells in series = 1 module, 2 modules installed in the battery
Potting material	Epoxy resin
Case material	Al
Dimension	168 mm × 102 mm × 99 mm
Weight	2.42 kg
Energy density	
Weight	70 Wh kg^{-1}
Volume	102.2 Wh L^{-1}

negative electrodes, which consisted of a mixture of graphite and binder coated onto a copper current collector (details of thicknesses, loading densities and porosities are proprietary). The liquid electrolyte was 1 M $LiPF_6$EC/DEC (3:7 by wt%) with a few weight percent additives. The cells were incorporated into a battery shown in Fig. 1(b), with the details given in Table 2. One module in the battery consisted of seven cells connected in series, with two modules connected in parallel. The cells were assembled in an aluminium casing filled with epoxy resin to ensure no solvent leakage during the low pressure orbital conditions. An electrical control circuit, with bypass circuits for each cell, was incorporated into the battery casing. The resulting battery was installed into the microsatellite REIMEI. Self-heating of the battery was used to bring the pack up to a temperature of 15 °C, with an onboard heater used to increase the temperature a further 5 ° to 20 °C. The voltage and the temperature of the battery were measured on a regular basis and logged in the control room at JAXA. The cycling conditions for the battery are shown in Table 3. The satellite experienced 33 min of eclipse during which time the battery met the electrical demands of the mission, resulting in 14 and 16% of the capacity discharged during measurements of the Auroral structures above the North and South Poles, respectively. The battery was recharged during the 63 min of sunshine with a constant current/constant voltage scheme (1.5 A/4.1 V). The operating voltage window for the battery was maintained between approximately 100 and 80% state-of-charge (SOC) in order to provide a backup energy supply in the case of emergency, and software and hardware undervoltage controls were used as safety measures in the case of battery over-discharge or failure.

Table 3
Terrestrial experimental simulation and orbital REIMEI battery conditions

	Terrestrial	North Pole	South Pole
Charge (CC/CV)	1.5A/4.1V 65min	1.5A/4.1V 63min	
Discharge (CC)	1.0A 35min	0.88A 15 min	0.78A 25min
		0.74A 18min	0.96A 5min
			1.6A 3min
ΔSOC	20%	14%	16%
Temperature			
Battery			
Eclipse	25°C	20°C	
Sunlight	25°C	20°C	
Solar panel			
Eclipse	-	-70°C	
Sunlight	-	140°C	

2.2. Terrestrial experimental simulations of the REIMEI battery

Terrestrial experimental simulations of a pouch cell and an identical copy of the REIMEI battery pack were undertaken with the forecasted satellite cycling and temperature conditions. The pouch cell and battery pack were cycled at 25 °C at atmospheric pressure inside a specially designed testing chamber where the temperature was controlled with a water cooling circuit (Advantec: TBG120AA Cooling Circulator). The cell/cells in the pack were discharged from a fully charged state with 1.0 A for 35 min, corresponding to a ΔSOC of 20%, followed by a constant current/constant voltage recharging scheme (1.5 A/4.1 V) for 65 min. The cell/cells in the pack were continuously cycled with no open circuit potential periods. The cycling conditions are shown in Table 3. The cycling was undertaken with a TOSCAT 5000 multichannel potentiostat controlled with TOSCAT 5000 software. The cell and pack were to be cycled until the end-of-discharge voltage was < 3.75 V, which corresponded to the 26.25 V hardware undervoltage control onboard REIMEI. The cycling was started prior to launching the satellite and continued during the duration of the mission. Subsequently, the terrestrial and orbital EODV performance as a function of cycle number was compared, and a calibration of the data undertaken to allow for slightly different discharge loads. The details of the calibration technique are reported elsewhere [13].

2.3. Accelerated ageing matrix

2.3.1. Beginning-of-life procedure

Pouch cells were received from the manufacturer and stored in a fully discharged state at 7 °C prior to lifetime measurements. The cells were slowly acclimatised to 25 °C and subjected to a series of reference performance tests, including capacity, DC resistance and impedance measurements, in order to characterise beginning-of-life (BOL) performance and to screen cells for selection into further lifetime testing. Cycling measurements were conducted using either a TOSCAT 5000 (6 channel) or TOSCAT 3000 (10 channel) multichannel potentiostat controlled with either TOSCAT 5000 or TOSCAT 3000 software, respectively. Impedance measurements were conducted with a PARSTAT 2263 Advanced Electrochemical System controlled with Electrochemistry Powersuite software. DC resistance measurements were conducted with an electronic load (Model PLZ 152 WA), a digital oscilloscope [Tektronix: TDS 2012 two channel(100 MHz, 1 GS s^{-1})], an amplifier (Tektronix: TCPA300, AC/DC current probe) and a multimeter (Agilent 34401A 6.5 Digit). The results from the DC resistance measurements were recorded with Excel Intuilink (Agilent Toolbar Utility) and Openchoice Desktop (Tektronix) Oscilloscope PC communications, 2500 data points in time (4 μs sampling rate). The details of the four reference performance tests are as follows:

- *C*/10 (0.3 A) charge and discharge capacity determination. From a fully charged condition (4.1 V), the cells were discharged with a constant current until the lower voltage limit (3 V) was reached, followed by 1 h at OCP condition. The cells were then recharged with a constant current/constant voltage scheme with a 4.1 V upper voltage limit and a total recharge time of 11 h, followed by 1 h at OCP condition. The cells were cycled twice with the same protocol.

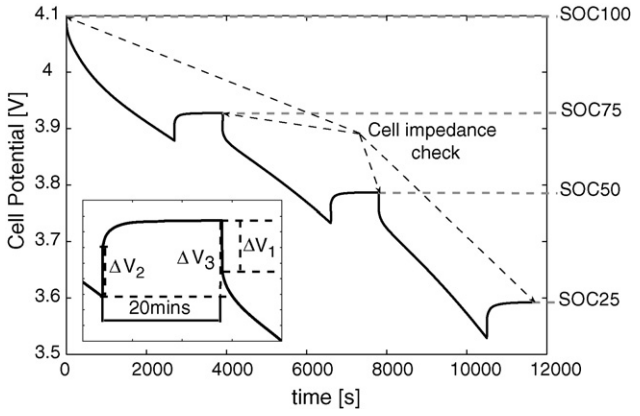

Fig. 2. Current interrupt measurement at four target SOCs (100, 75, 50, 25%) with a $C/3$ (1.0 A) discharge current between the cell voltage limits (4.1–3.0 V); inset showing the different ΔV measurements: ΔV_1—potential drop when the discharge load was applied, ΔV_2—potential relaxation when the current load was removed, and ΔV_3—total potential relaxation after a 20 min resting period.

- $C/3$ (1.0 A) discharge and $C/2$ (1.5 A) charge capacity determination using the same cycling protocol as the $C/10$ capacity check, with the total recharge time reduced to 4 h.
- Combined current interrupt/potential relaxation test at multiple SOCs (refer to Fig. 2). From a fully charged condition (4.1 V), the cells were discharged with a $C/3$ current (1.0 A) for the period of time necessary to remove 25% of the capacity (based on the $C/3$ discharge capacity test), followed by 20 min at OCP condition. The potential drop when the discharge load was applied, ΔV_1, and the potential relaxation when the load was removed, ΔV_2, were measured with an oscilloscope. Furthermore, the total potential relaxation after a 20 min relaxation period, ΔV_3, was measured with a multimeter. The measurement was repeated at four SOCs: 100, 75, 50 and 25%.
- Impedance was measured at four target SOCs (100, 75, 50 and 25%) as a part of the combined current interrupt/potential relaxation measurement given above (refer to Fig. 2). After discharging 25% of the capacity and measuring ΔV_1, ΔV_2 and ΔV_3, the cell was left at an open circuit condition for a further 40 min, resulting in a total of 1 h relaxation time prior to the impedance measurement. The impedance was measured potentiostatically around this final OCP condition with a 5 mV amplitude either for the frequencies 100 kHz to 0.5 mHz (50 points, logarithmic spacing, quality 2) or 100 kHz to 10 mHz (65 points, logarithmic spacing, quality 2).

2.3.2. General set-up

The pouch cells that successfully completed the initial reference performance tests were placed into a temperature chamber (Advantec: TBG120AA Cooling Circulator for 25 °C measurements, ESPEC: Model PU-2KT for 45 °C measurements) with the positive and negative terminals contacted by cables reinforced with masking tape. The pouch cells were connected to either a TOSCAT 5000 (6 channel) or TOSCAT 3000 (10 channel) multichannel potentiostat controlled with either TOSCAT 5000 or TOSCAT 3000 software, respectively. Accelerated cycling tests were undertaken at two DODs (20, 40%) and two temperatures (25, 45 °C) at atmospheric pressure. Details of the lifetime matrix are given in Table 4. Reference performance tests, identical to the tests at beginning-of-life, were undertaken every 400 cycles at 25 °C, which corresponded to approximately 28 days. In addition to the cycling tests, two cells were placed under calendar conditions at SOC 100% and 25 °C.

2.3.3. Cycling cells

The cells were continuously cycled with a LEO regime in an upper SOC-window (i.e. between either 100–80% SOC or 100–60% SOC), including a 35 min constant current discharge (1.0 A for ΔDOD 20% and 2.0 A for ΔDOD 40%) and a 65min constant current/constant voltage recharging scheme with 1.5 A and a 4.1 V upper voltage limit. The different components of the lifetime matrix were started at different times, resulting in 4800 completed cycles at 25 °C DOD 20%, 3400 completed cycles at 25 °C DOD 40%, and 1600 completed cycles for both discharge current loads at 45 °C. Two cells were tested at all conditions except for 25 °C DOD 40%, where six cells were used to allow for frequent removal of cells from testing for disassembly. During the 1 year of lifetime testing at JAXA, two cells were removed from the 25 °C DOD 40% tests (after 1200 and 2200 completed cycles) and one cell was removed after 1200 completed cycles from 45 °C DOD 20% and 45 °C DOD 40% tests.

2.3.4. Calendar cells

Two pouch cells were charged to 4.1 V and allowed to float at this condition at 25 °C for 1 year. The calendar life test was started at the same time as the 25 °C DOD 40% tests, and a series of reference performance tests were undertaken at the corresponding completion of 2800 and 3400 cycles. In addition to the four normal reference performance tests, the self-discharge (i.e. difference between the initial and remaining capacity) of the battery was measured by discharging the battery to the lower voltage limit of 3.0 V with a $C/3$ (1.0 A) constant current.

3. Results

3.1. Comparison of terrestrial and orbital battery performance

A comparison between the performance of the REIMEI battery in orbit and of both a pouch cell and an identical copy of the REIMEI battery pack experimentally simulated with the forecasted satellite cycling and temperature conditions is shown in Fig. 3. A comparison between the terrestrial and orbital cycling conditions is shown in Table 3. The charge conditions were similar for both cases, however, the discharge conditions were quite different with respect to both duration and current load. The difference in the current loads was due to the use of the onboard camera in different modes to observe Aurora above either the North or South Pole. In particular, observations above the South Pole (between ~ 4000 and 6000 completed cycles) included a 1.6 A load towards the end of dis-

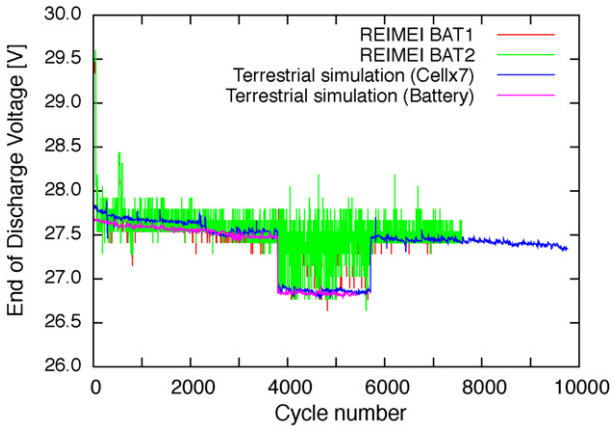

Fig. 3. Calibrated terrestrial cycling data comparison with REIMEI orbital data. (For interpretation of the references to colour in this figure legend, the reader is referred to the web version of the article.)

Table 4
3 Ah battery lifetime test matrix

Temperature (°C)	Pressure (kPa)	No. of cells			Frequency of performance tests	End of life criterion
		Cycling		Calendar		
		DOD 20%	DOD 40%	floating		
25	101.325	2	6	2	Every 400 cycles (28 days)	End of cycling discharge voltage < 3.75 V
45	101.325	2	2	–	Every 400 cycles	As above

charge, resulting in the significant decrease in EODV shown in Fig. 3. In order to compare the terrestrial and orbital results, a detailed calibration of the data was undertaken and reported elsewhere [13]. A comparison of the results indicated that the lithium-ion cells in the REIMEI pack were not inadvertently affected by the conditions of space. In addition, the good agreement of the data allowed terrestrial experimental results to be used to both predict battery lifetime onboard the satellite and provide feedback on cell state-of-health by conducting lifetime investigations incorporating reference performance tests. In addition to the electrochemical performance, the temperature of the battery pack was monitored and found to be successfully maintained at ~20 °C despite the fact that the surface temperature of the solar panels was between −70 and 140 °C during periods of eclipse and sunlight, respectively. The successful management of the battery temperature was primarily attributed to the engineering design of the satellite, which included segments of either conductive (SSM) or insulating (MLI) panels.

3.2. Lifetime matrix: 3 Ah pouch cell performance

3.2.1. Capacity fade

The impact of temperature (25, 45 °C), depth-of-discharge (20, 40%) and cycling on the $C/3$ (1.0 A) discharge capacity (4.1–3.0 V) as a function of cycle number is shown in Fig. 4(a). A comparison of the results at 25 °C revealed that the depth-of-discharge had a small impact on the capacity fade. In addition, increasing the temperature to 45 °C whilst maintaining the depth-of-discharge at 20% had a similar impact on the capacity fade as increasing the depth-of-discharge to 40% at 25 °C. The most significant impact on the capacity fade was observed when an increase in the temperature to 45 °C was coupled with an increase in the depth-of-discharge to 40%. After remaining at float conditions for approximately nine months (2800 completed cycles for 25 °C DOD 40%), the calendar cells had self-discharged approximately 28% of the original $C/3$ capacity, with approximately 5% representing an irreversible loss. The average capacity fade of the calendar, 25 °C DOD 20% and 25 °C DOD 40% cells after approximately nine months of ageing was 5.48, 17.13 and 18.83%, respectively. These data indicate that cycling accelerated cell capacity fade.

Prediction of cell life based on the $C/3$ discharge capacity was undertaken on the two ageing cases reflecting realistic conditions onboard a satellite (i.e. 25 °C DOD 20% and 25 °C DOD 40%). The capacity fade results, shown in Fig. 4(a), were plotted as a function of the square root of the cycle number, with the resulting curves shown in Fig. 4(b). A linear relationship was fitted to both sets of data and extrapolated (assuming the linear relationship was valid for the duration of cell life) to the target cycle lifetime of 30 000 continuous LEO cycles. The results were similar for both depths-of-discharge, with an approximately 60% decrease in capacity. This approach to predicting cell life is common in the battery community and implicitly assumes that the main source of capacity fade is the irreversible consumption of lithium ions at the negative electrode. However, as discussed in Part two [14], the capacity fade mechanism of $Li_xMn_2O_4$-based batteries is complicated and difficult to attribute to one source alone. Therefore, these results serve both as a rough guide and a base of comparison with other battery technologies for LEO satellite application.

The cycling curves for the two cases [25 °C calendar life (equivalent of 3400 completed LEO cycles) and 45 °C DOD 40% 1600 completed cycles] representing the two extremes of capacity fade using both a low ($C/10$) and high ($C/3$) current are shown in Fig. 5(a) and (b), respectively. The hysteresis observed with a low current was exaggerated with a higher current for all cases due to the cell impedance, with an increase in the degree of the hysteresis effect for the cell cycled with a 40% depth-of-discharge at 45 °C. Comparison of the cycling curves for the fresh cell with the calendar cell revealed very little difference in the shape of the curves at each current load, with a disappearance of the characteristic spinel inflections at the higher current whilst maintaining the same

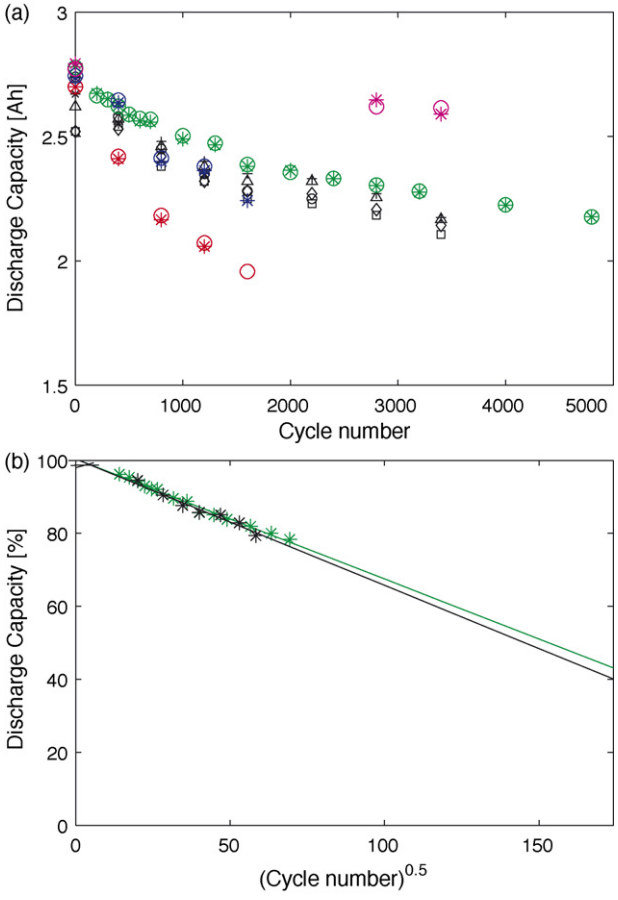

Fig. 4. Capacity measured at 25 °C with a $C/3$ (1.0 A) discharge current (4.1–3.0 V): (a) full cell (3 Ah) capacity fade, (b) percentage of original $C/3$ capacity plotted versus the square root of the cycle number, with a linear relationship fitted and extrapolated to 30 000 LEO cycles; (green) 25 °C DOD 20%, (black) 25 °C DOD 40%, (blue) 45 °C DOD 20%, (red) 45 °C DOD 40%, (magenta) 25 °C calendar life (fully charged under float conditions) [note: the different cells tested at each condition are indicated with a symbol]. (For interpretation of the references to colour in this figure legend, the reader is referred to the web version of the article.)

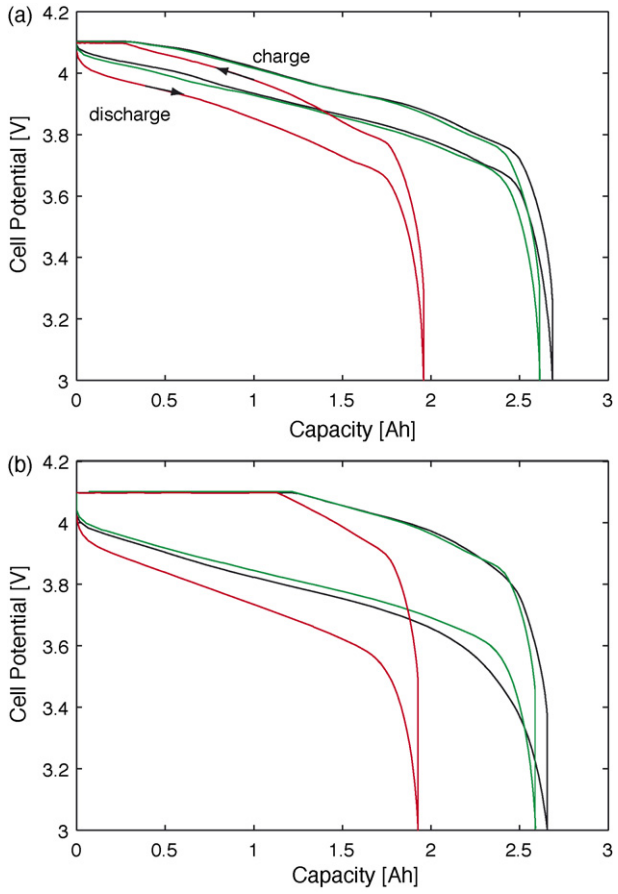

Fig. 5. Cycling (3.0–4.1 V) of fresh and aged 3 Ah pouch cells: (a) C/10 (0.3 A) cycling, (b) C/3 (1.0 A) discharge, C/2 (1.5 A) charge; (black) fresh, (green) 25 °C calendar life (equivalent of 3400 completed LEO cycles), (red) 45 °C DOD 40% 1600 completed cycles. Direction of charge/discharge illustrated with black arrows in (a). (For interpretation of the references to colour in this figure legend, the reader is referred to the web version of the article.)

capacity. The largest difference was observed when the cell was cycled with a large depth-of-discharge at a higher temperature, resulting in a significant decrease in the capacity at both current loads. However, the same capacity was obtained regardless of the current with similar cycling profiles to the other two cells.

3.2.2. End-of-Discharge-Voltage versus cycle number

The impact of temperature (25, 45 °C) and depth-of-discharge (20, 40%) on both the EODV and average discharge energy as a function of cycle number is shown in Fig. 6(a) and (b), respectively. As expected, the EODV at a particular depth-of-discharge was generally higher at 45 °C due to a lower cell resistance at a higher testing temperature. A comparison of the effect of depth-of-discharge at 25 °C revealed similar behaviour, with the rate of decrease in the EODV during the first ~ 1500 cycles reducing during subsequent cycles. In addition, the average discharge energy was almost twice as large for 40% depth-of-discharge. An examination of the effect of temperature revealed that there was almost no difference at 20% depth-of-discharge but a significant difference at 40% depth-of-discharge. The combination of both a higher depth-of-discharge (40%) and a higher temperature (45 °C) accelerated the performance degradation of the cell.

3.2.3. Impedance

The impedance of the cells aged in the lifetime matrix was measured regularly at four SOCs (100, 75, 50 and 25%) at 25 °C. For clarity, the results at a high (100%) and a low (25%) SOC are examined and shown in Figs. 7 and 8, with the results for frequencies greater than 1000 Hz removed due to an experimental artefact.

In general, the impedance spectra measured for all ageing conditions indicated that the increase in the impedance was small and mainly concentrated in the high-frequency region. The lack of change of the low-frequency impedance for cells aged with a 40% depth-of-discharge at either 25 or 45 °C is demonstrated in Figs. 9(a) and (b), respectively. Figs. 7(a) and 8(a) for cells aged at 25 °C with a 20% depth-of-discharge revealed very little change in the width of the high-frequency semi-circle at 100% SOC and both a noticeable increase in the width of and development of a second bump in the high-frequency semi-circle at 25% SOC. Similar behaviour was observed when the temperature was increased to 45 °C after a smaller number of cycles (1600 vs. 4800 at 25 °C), see Figs. 7(c) and 8(c), but an additional change was observed in the high-frequency real axis intercept which increased noticeably for both 100 and 25% SOC. Increasing the cycling depth-of-discharge to 40% generally resulted, see Figs. 7(b) and (d) and 8(b) and (d), in a slightly larger high-frequency semi-circle and an observed shift in the high-frequency real axis intercept regardless of the testing temperature. The SOC-dependence of the measured impedance observed for cells cycled with a 20% depth-of-discharge was observed for cells cycled with a 40% depth-of-discharge, with the cells exhibiting an increase in the width of the high-frequency semi-circle and the appearance of a second bump at 25% SOC. In addition to observing changes in the magnitude of the impedance as a function of cycle number under different testing temperatures

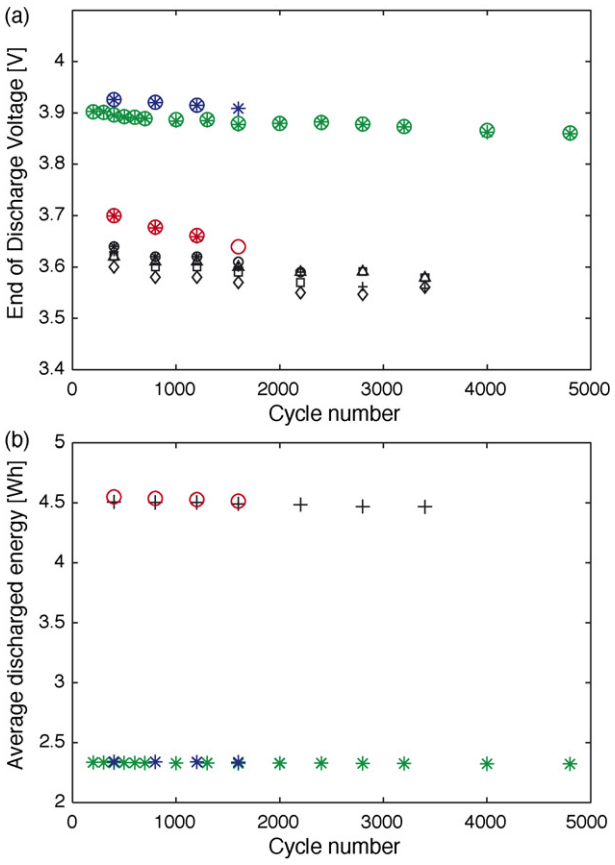

Fig. 6. Full cell (3 Ah) performance: (a) end-of-discharge-voltage (EODV), (b) average discharged energy; (green) 25 °C DOD 20%, (black) 25 °C DOD 40%, (blue) 45 °C DOD 20%, (red) 45 °C DOD 40%. (For interpretation of the references to colour in this figure legend, the reader is referred to the web version of the article.)

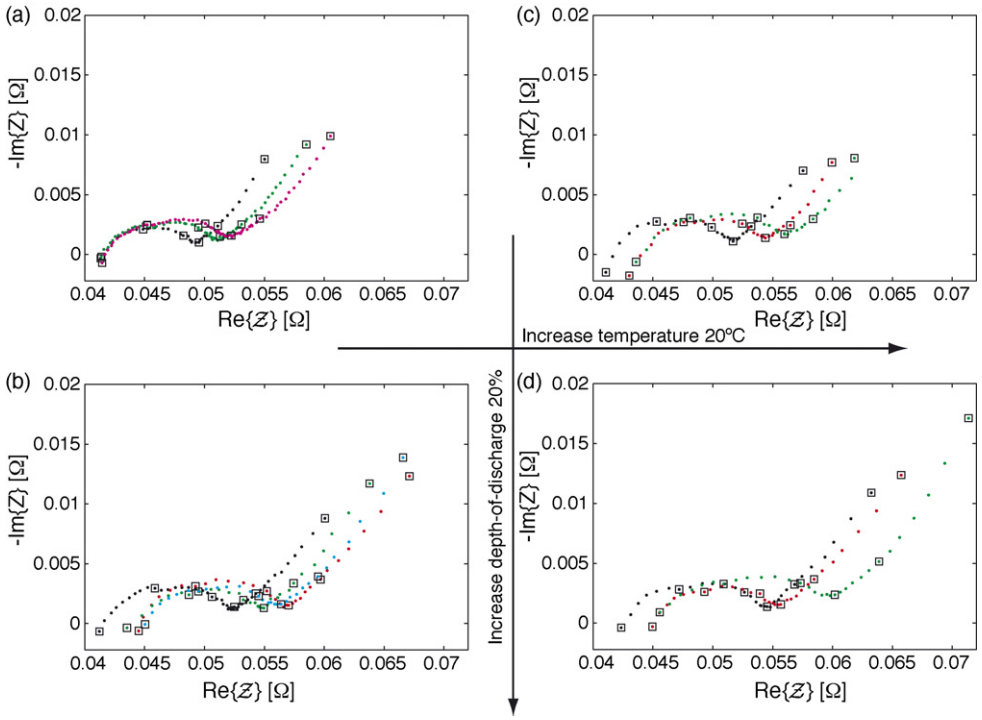

Fig. 7. Impedance of cells aged with various conditions; measurement point: SOC 100%; impedance from 1000 Hz to 10 mHz; (•) BOL, (●) 800, (●) 1600 cycles, (●) 3400, (●) 4800: (a) 25 °C DOD 20%, (b) 25 °C DOD 40%, (c) 45 °C DOD 20%, (d) 45 °C DOD 40%. Each decade in frequency indicated with □. (For interpretation of the references to colour in this figure legend, the reader is referred to the web version of the article.)

and depths-of-discharge, it was important to investigate any shifts in the frequency at which different characteristic features of the Nyquist plot were observed. In particular, a possible change in the frequency at which the intersection between the high-frequency semi-circle and the low-frequency diffusion tail, defined as *fmin* in other work [15], was examined. Approximately each decade change of frequency is indicated in Figs. 7 and 8, with the frequency of *fmin* observed to remain the same regardless of the testing condition or

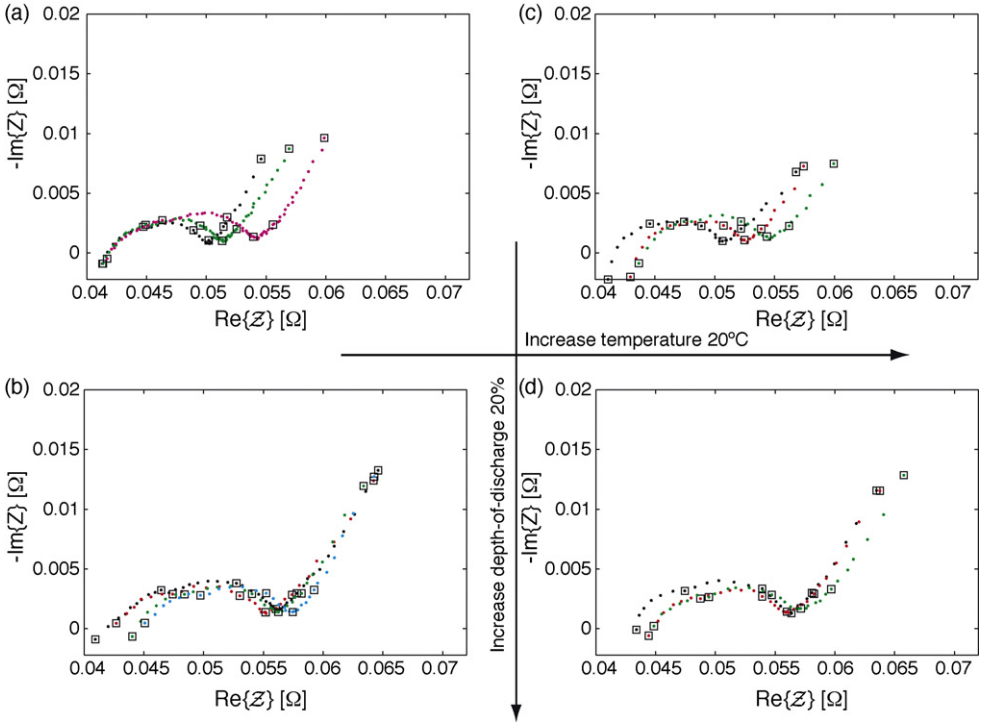

Fig. 8. Impedance of cells aged with various conditions; measurement point: SOC 25%; impedance from 1000 Hz to 10 mHz; (•) BOL, (●) 800, (●) 1600 cycles, (●) 3400, (●) 4800: (a) 25 °C DOD 20%, (b) 25 °C DOD 40%, (c) 45 °C DOD 20%, (d) 45 °C DOD 40%. Each decade in frequency indicated with □. (For interpretation of the references to colour in this figure legend, the reader is referred to the web version of the article.)

cycle number. This result differed in comparison with the lifetime observations for nickelate-based chemistry [15].

3.2.4. Direct resistance

Current interrupt measurements were regularly undertaken on the cells aged in the lifetime matrix in order to obtain ΔV_1 (100, 75 and 50% SOC), ΔV_2 (75, 50 and 25% SOC) and ΔV_3 (75, 50 and 25% SOC), as defined in Fig. 2. The purpose of the measurements was to investigate if any of these quantities could potentially be used as an on-board SOH indicator. The change in the cell potential after either the application (ΔV_1) or removal (ΔV_2) of a 1.0 A ($C/3$) load was measured with an oscilloscope, with an example of the data shown in Fig. 10. The data obtained both before and after the current interrupt was fitted with a linear relationship (equal amount of data points) and the expression prior to the interrupt extrapolated to a point in time corresponding to the first fitted point after the interrupt (see Fig. 10). The difference in the cell potential was divided by the current load in order to obtain the resistance. For clarity, the results obtained for the cells aged with a 40% depth-of-discharge cycle at both 25 and 45 °C are examined since these cells had the most noticeable change in the full cell impedance. The increase in the resistance as a function of cycle number after either the application or removal of the current load are shown in Fig. 11(a) and (b), respectively. Although the measurements for the two cells aged at 45 °C revealed that there was some scatter in the data, in general there was no clear dependence of either resistance on the SOC. In addition, the relationship between the resistance and the cycle number could be approximated with a linear equation for both cases, with the slope for the cells aged at 45 °C larger than for the cells aged at 25 °C. Measuring the change in the cell potential with the accuracy of an oscilloscope onboard the satellite could be impractical, therefore the change in the cell potential at the end of a 20 min OCP period after the removal of the current load was measured and shown in Fig. 11(c). Unfortunately, both the scatter in the data and a total lack of a linear relationship between ΔV_3 and cycle number made this measured quantity a poor candidate for SOH indication.

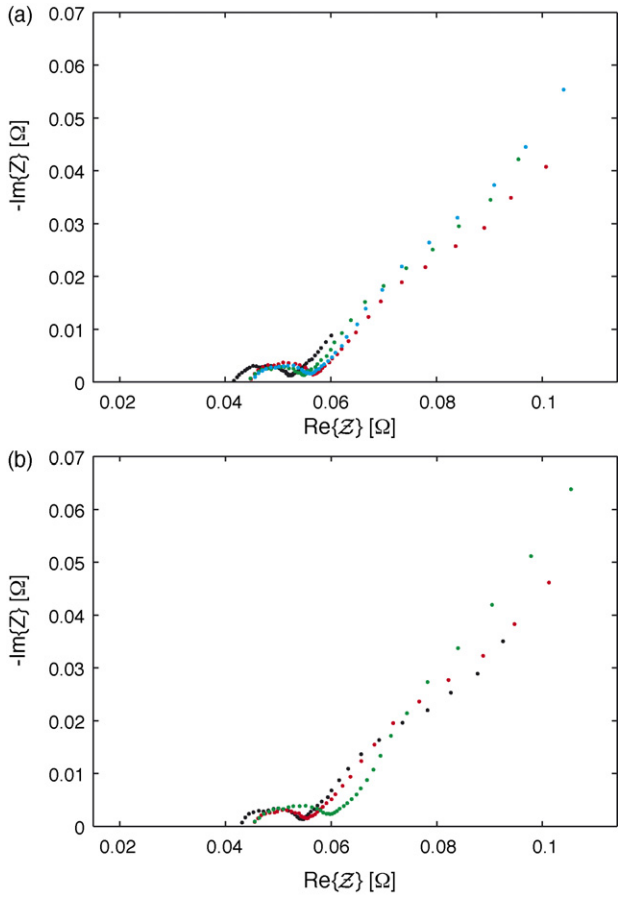

Fig. 9. Impedance of cells aged with a DOD 40% LEO satellite cycle: (a) 25 °C, (b) 45 °C; measurement point: SOC 100%; impedance from 1000 Hz to 0.5 mHz; (•) BOL, (●) 800 cycles, (●) 1600 cycles, (●) 3400 cycles [note: BOL cell impedance (•) in (a) measured from 1000 Hz to 10 mHz]. (For interpretation of the references to colour in this figure legend, the reader is referred to the web version of the article.)

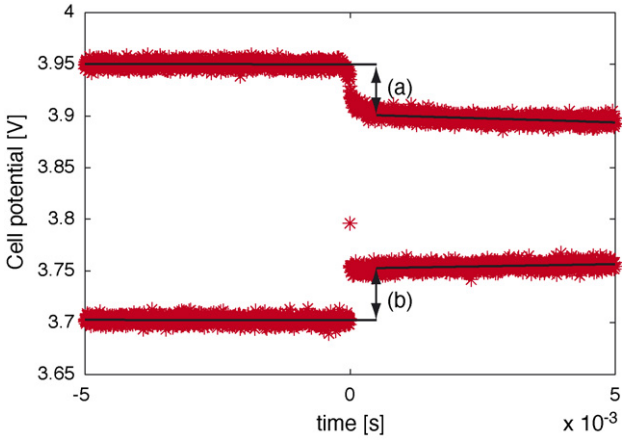

Fig. 10. Diagram of the analysis of the current interrupt data: (a) estimated decrease in the cell potential (ΔV_1) after the application of a constant $C/3$ (1.0 A) discharge current, and (b) estimated increase in the cell potential (ΔV_2) after removing 25% of the capacity with a constant $C/3$ (1.0 A) discharge current.

There are no clear guidelines as to how a prognostic SOH indication scheme should be designed. For LEO satellites, where moderately low currents are used with high-energy designed cells, the SOH indicator could be based on an estimation of the remaining $C/3$ discharge capacity between the cell potential limits (4.1–3.0 V). This approach to SOH indication required establishment of a relationship between a measurable quantity onboard the satellite, for example, ΔV_1, and the discharge capacity. When the capacity fade results, shown in Fig. 4, were plotted as a function of the square root of the cycle number the resulting curves were linear. Combining this knowledge with the linear relationship between the discharge resistance from a fully charged condition (i.e. SOC 100%) and the cycle number, it was possible to plot the resistance versus the inverse of the discharge capacity squared and obtain a linear relationship that is shown Fig. 12. Although not shown, the same linear relationship existed independent of the testing SOC (i.e. 100, 75 and 50%) with a focus on 100% SOC in this work due to practical considerations onboard a satellite. The fact that the measured points for both 25 and 45 °C result in the same slope of the linear relationship provided both confidence in using the higher temperature as an accelerating factor and a relationship that was valid in this temperature range. An extension of the current lifetime matrix to lower temperatures and a longer testing period would provide the data necessary to both further improve the confidence in the linear relationship and increase the feasibility of this approach for SOH indication.

4. Discussion

The analysis of performance data for 3 Ah pouch cells aged with a LEO cycling regime in a lifetime matrix of three depths-of-discharge (0, 20 and 40%) and two temperatures (25 and 45 °C)

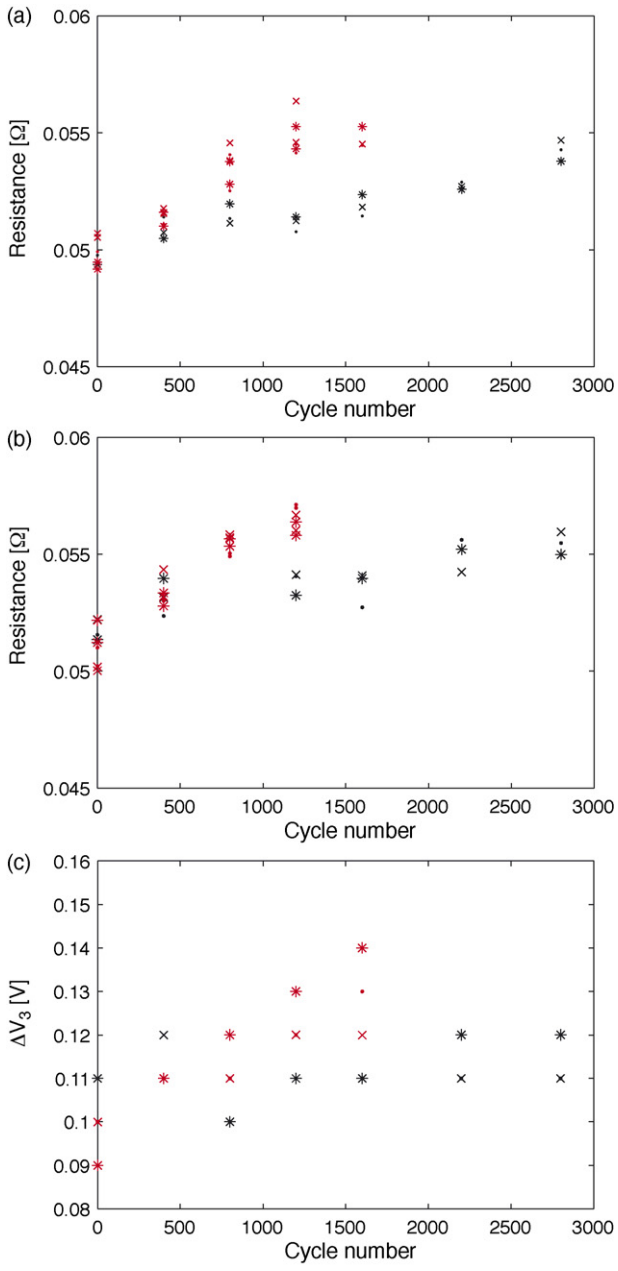

Fig. 11. Current interruption measurements (constant $C/3$ (1.0 A) discharge current at 25 °C) of cells aged with a LEO DOD 40% cycle at two temperatures: (black) one cell at 25 °C and (red) two cells at 45 °C: (a) resistance upon application of the current load (ΔV_1) at three SOCs: (•) 100%, (∗) 75%, and (×) 50%, (b) resistance upon removal of the current load (ΔV_2) at three SOCs: (•) 75%, (∗) 50%, and (×) 25%, (c) increase in the potential (ΔV_3) 20 min after removal of the current load at three SOCs: (•) 75%, (∗) 50%, and (×) 25%. (For interpretation of the references to colour in this figure legend, the reader is referred to the web version of the article.)

led to several important observations. Firstly, increasing both the depth-of-discharge by 20% and the temperature by 20 °C from the REIMEI base case (25 °C DOD 20%) had a clear impact on the degradation of the $C/3$ discharge capacity and EODV, as shown in Figs. 4 and 6, respectively. In general, higher temperatures and larger depths-of-discharge are associated with an accelerated capacity fade for this electrode chemistry [16,11,17]. The only other published lifetime investigation of a $Li_xMn_2O_4$-based battery for LEO satellites focussed on a 20% depth-of-discharge at 15 °C and reported the EODV as a function of cycle number [8], with the cells tested in this study having comparable performance. Comparison of both the capacity fade and EODV results for cells (25 °C DOD 40%) in this study with different cell chemistries aged with similar conditions revealed comparable results [18,19]. However, an improved performance was observed for cells based on iron phosphate chemistry [19].

Secondly, impedance measured for all ageing conditions indicated that the increase was small, manifested in a SOC-dependent increase of the high-frequency semi-circle and a noticeable increase in the high-frequency real axis intercept at both higher depths-of-discharge and temperatures. A change in the shape and magnitude of the high-frequency semi-circle could be attributable to changes in the surface properties of the active material, conductive fillers or current collectors in either/both composite porous electrodes. In addition, an increase in the high-frequency real axis intercept could indicate a degradation of electrode tabbing, contact problems between either conductive particles and/or the conductive particles and the current collector in either/both composite porous electrodes, a degradation of the electrolyte properties or a decrease of the separator porosity. The very small change in the impedance, even at higher temperatures, was impressive in comparison with similar measurements of $LiCoO_2$-based lithium-ion batteries aged with a 40% depth-of-discharge LEO cycling profile [7,2,10]. These impedance results indicated that as long as the capacity fade of the 3 Ah cells is minimised, the battery chemistry should provide a stable EODV for the mission duration onboard the satellite.

Thirdly, the impact of increasing the depth-of-discharge to 40% at the temperature condition onboard REIMEI (25 °C) was investigated in order to evaluate this load for future piggy-back missions. Increasing the depth-of-discharge to 40% could potentially decrease the battery weight and represent the opportunity to increase satellite payload. Capacity fade and performance degradation were not seen to increase significantly by increasing the depth-of-discharge. But, the extrapolated $C/3$ discharge capacity at 30 000 completed LEO cycles equalled the capacity required during a 40% load, i.e. discharging by DOD 40% at 30 000 cycles would completely drain the battery. However, the battery could be used for shorter durations, such as a 1 or 2 year piggy-back mission, at the higher load. Although the average $C/3$ discharge energy was twice as high for the higher depth-of-discharge, see Fig. 6(b), the EODV was noticeably lower, see Fig. 6(a). Therefore, in order for this current load

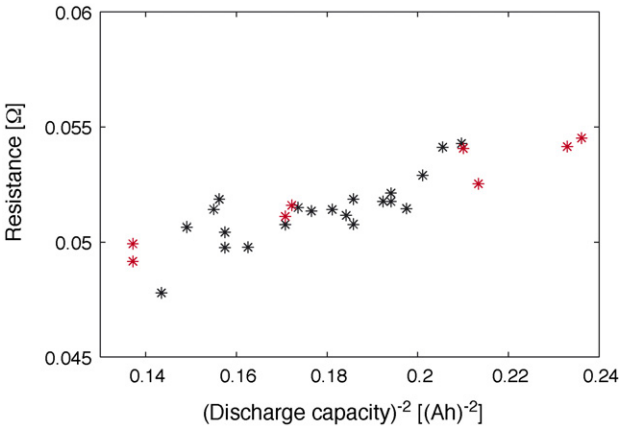

Fig. 12. Relationship between the resistance of the cell (discharged with a $C/3$ (1.0 A) current) and the discharge capacity ($C/3$; 4.1–3.0 V) at 25 °C; decrease in the potential (ΔV_1) measured with an oscilloscope at SOC 100%; cells aged with a LEO DOD 40% cycle at two temperatures: (black) three cells at 25 °C and (red) two cells at 45 °C. (For interpretation of the references to colour in this figure legend, the reader is referred to the web version of the article.)

to be used onboard REIMEI, both the undervoltage controls and end-of-life criteria would need to be revised.

The overall objectives of this study were to provide a better understanding of the lifetime performance of commercial laminated $Li_xMn_2O_4$-based lithium-ion batteries for LEO applications and demonstrate the value of taking a two-tiered approach to battery lifetime studies. The use of electrochemical impedance spectroscopy to probe the effects of ageing at different SOCs proved to be an invaluable tool at the full cell (3 Ah) level. However, in order to interpret both the full cell capacity and impedance results, the two-tiered approach must be extended to include two- and three-electrode electrochemical examination of both positive and negative electrodes harvested in a controlled environment (e.g. dry room or glove box) at different points of ageing. The current generation of 3 Ah cells used in this study were observed to perform well onboard REIMEI, with a comparison of the terrestrial reference performance test results with other battery chemistries indicating that this battery chemistry should be considered for future satellite missions.

5. Conclusions

The low-earth-orbit cycle life performance of commercial 3 Ah laminated $Li_xMn_2O_4$-based lithium-ion batteries has been investigated under both orbital and terrestrial conditions. A terrestrial lifetime matrix of different cycling DODs (0, 20, 40%) and temperatures (25, 45 °C) was undertaken with periodic reference performance tests. The following points summarise the main conclusions of this study:

(1) The battery pack onboard REIMEI was not inadvertently affected by the conditions of space. Furthermore, the good agreement of the orbital and terrestrial data allowed terrestrial experimental results to be used to both predict battery lifetime onboard the satellite and provide feedback on cell state-of-health by conducting lifetime investigations incorporating electrochemical reference performance tests.
(2) Lifetime studies of 3 Ah cells revealed that increasing either the depth-of-discharge by 20% or the temperature by 20 °C from the REIMEI base case (DOD 20%, 25 °C) had little impact on the degradation of the C/3 discharge capacity and EODV. However, a simultaneous increase of temperature (to 45 °C) and depth-of-discharge (to 40%) significantly increased cell capacity fade. Furthermore, impedance spectra measured for all ageing conditions indicated that the increase was small, manifested in a SOC-dependent increase of the high-frequency semi-circle and a noticeable increase in the high-frequency real axis intercept at both higher depths-of-discharge and temperatures.
(3) Comparison of the lifetime performance of 3 Ah cells aged with either cycling or calendar (SOC 100%, float conditions at 25 °C) conditions indicated that cycling had a significant impact on the capacity fade. Furthermore, calendar cells left to continuously float for a nine month period were found to self-discharge approximately 28% of their initial C/3 capacity, with approximately 23% of this effective capacity loss recoverable upon recharging.
(4) Using the current interrupt technique, a linear relationship was observed between a resistance based on the immediate potential drop upon an application of a current load (25 °C) and cycle number, which led to the formulation of a relationship between resistance and capacity fade valid for cells aged at both 25 and 45 °C. This observed linear relationship possibly indicated that the ageing mechanism was the same at both room and elevated temperatures, validating temperature as a useful tool when accelerating the degradation of this particular chemistry. In addition, the linear relationship potentially provided a basis for a prognostic SOH indicator.

Acknowledgements

Financial support from the Swedish Governmental Agency for Innovation Systems (VINNOVA; Green Car Project) and the Japan Aerospace Exploration Agency (JAXA) is gratefully acknowledged. Shelley Brown would like to thank Yoshitsugu Sone, Keita Ogawa and Masatoshi Uno for providing the resources and support necessary to undertake the lifetime work at JAXA.

References

[1] M.C. Smart, B.V. Ratnakumar, L.D. Whitcanack, K.B. Chin, S. Surampudi, R. Gitzendanner, F. Puglia, J. Byers, IEEE AESS Syst. Mag. (2004) 18.
[2] X. Wang, C. Yamada, H. Naito, S. Kuwajima, J. Power Sources 140 (2005) 129.
[3] H. Yoshida, N. Imamura, T. Inoue, K. Komada, Electrochemistry (Tokyo, Jpn.) 71 (2003) 1018.
[4] R.A. Marsh, S. Vukson, S. Surampudi, B.V. Ratnakumar, M.C. Smart, M. Manzo, P.J. Dalton, J. Power Sources 97–98 (2001) 25.
[5] J.P. Fellner, G.J. Loeber, S.P. Vukson, C.A. Riepenhoff, J. Power Sources 119-121 (2003) 911.
[6] Y. Sone, X. Liu, T. Inoue, X. Wang, S. Kuwajima, Electrochemistry, (Tokyo, Jpn.) 71 (2003) 542.
[7] X. Wang, Y. Sone, S. Kuwajima, J. Power Sources 142 (2005) 313.
[8] X. Wang, Y. Sone, H. Naito, C. Yamada, G. Segami, K. Kibe, J. Power Sources 161 (2006) 594.
[9] B. McKissock, C. Reid, M. Manzo, T. Miller, D. Britton, W. Bennett, in: M. Anderman (Ed.), Second International Symposium on Large Lithium Ion Battery Technology and Application, 2006.
[10] X. Wang, Y. Sakiyama, Y. Takahashi, C. Yamada, H. Naito, G. Segami, T. Hironaka, E. Hayashi, K. Kibe, J. Power Sources 167 (2007) 162.
[11] T. Inoue, M. Sano, J. Electrochem. Soc. 145 (1998) 3704.
[12] G.G. Amatucci, A. Blyr, C. Sigala, P. Alfonse, J.M. Tarascon, Solid State Ionics 104 (1997) 13.
[13] K. Ogawa, Y. Takeda, S. Brown, M. Uno, Y. Sone, K. Tanaka, K. Hirose, M. Tajima, H. Saito, Electrochemistry (Tokyo, Jpn.), submitted for publication.
[14] S. Brown, K. Ogawa, Y. Kumeuchi, S. Enomoto, M. Uno, Y. Sone, D. Abraham, G. Lindbergh, J. Power Sources 185 (2008) 1454.
[15] D.P. Abraham, E.M. Reynolds, P.L. Schultz, A.N. Jansen, D.W. Dees, J. Electrochem. Soc. 153 (2006) 1610.
[16] A. Blyr, C. Sigala, G. Amatucci, D. Guyomard, Y. Chabre, J.-M. Tarascon, J. Electrochem. Soc. 145 (1998) 194.
[17] G.G. Amatucci, N. Pereira, T. Zheng, J.-M. Tarascon, J. Electrochem. Soc. 148 (2001) 171.
[18] T. Inoue, N. Imamura, H. Yoshida, K. Komada, NASA Aerospace Battery Workshop, Huntsville, USA, 2006.
[19] L. Lee, G.M. Rao, NASA Aerospace Battery Workshop, Huntsville, USA, 2006.